Available online at www.sciencedirect.com
SCIENCE DIRECT®
J. Chem. Thermodynamics 35 (2003) 919–937
JCT
www.elsevier.com/locate/jct

Heat capacities, third-law entropies and thermodynamic functions of the negative thermal expansion materials, cubic α-ZrW_2O_8 and cubic $ZrMo_2O_8$, from $T = (0$ to $400)$ K

Rebecca Stevens [a], Jessica Linford [a], Brian F. Woodfield [a], Juliana Boerio-Goates [a,*], Cora Lind [b,1], Angus P. Wilkinson [b], Glen Kowach [c]

[a] *Department of Chemistry and Biochemistry, Brigham Young University, Provo, UT 84602, USA*
[b] *School of Chemistry and Biochemistry, Georgia Institute of Technology, Atlanta, GA 30332, USA*
[c] *Bell Laboratories, Lucent Technologies, 600 Mountain Avenue, Murray Hill, NJ 07974, USA*

Received 24 September 2002; accepted 30 January 2003

Abstract

The molar heat capacities of crystalline cubic α-ZrW_2O_8 and cubic $ZrMo_2O_8$ have been measured at temperatures from (0.6 to 400) K. At $T = 298.15$ K, the standard molar heat capacities are (207.01 ± 0.21) $J \cdot K^{-1} \cdot mol^{-1}$ for the tungstate and (210.06 ± 0.42) $J \cdot K^{-1} \cdot mol^{-1}$ for the molybdate. Thermodynamic functions have been generated from smoothed fits of the experimental results. The standard molar entropies for the tungstate and molybdate are (257.96 ± 0.50) $J \cdot K^{-1} \cdot mol^{-1}$ and (254.3 ± 1) $J \cdot K^{-1} \cdot mol^{-1}$, respectively. The uncertainty of the entropy of the cubic $ZrMo_2O_8$ is larger due to the presence of small chemical and phase impurities whose effects cannot be corrected for at this time. The heat capacities of the negative thermal expansion materials have been compared to the weighted sums of their constituent binary oxides. Both negative thermal expansion materials have heat capacities which are significantly greater than the sum of the binary oxides over the entire temperature region.

* Corresponding author. Tel.: 1-801-378-2302; fax: 1-801-378-5474.
E-mail address: boerio-goates@byu.edu (J. Boerio-Goates).
[1] Present address: Department of Chemistry & Chemical Biology, Baker Laboratory, Cornell University, Ithaca, NY 14853.

0021-9614/03/$ - see front matter © 2003 Elsevier Science Ltd. All rights reserved.
doi:10.1016/S0021-9614(03)00050-8

Keywords: Negative thermal expansion materials; Heat capacity; Entropy; Thermodynamic functions

1. Introduction

A family of materials with structures related to that of cubic ZrW_2O_8 has been shown to exhibit negative thermal expansion (NTE) over a wide temperature range [1–3]. Other family members include HfW_2O_8 [1], $HfMo_2O_8$ [4], $ZrMo_2O_8$ [5], and the solid solutions of $Zr_{1-x}Hf_xW_2O_8$ [6] and $ZrW_{2-x}Mo_xO_8$ [7]. Materials that exhibit NTE behavior are of interest because of the potential to couple them with materials that exhibit positive thermal expansion to create composites whose thermal expansion properties can be finely tuned.

ZrW_2O_8 is the most widely studied member of this family. Below $T = 448$ K it exists in a cubic structure, designated α-ZrW_2O_8, that belongs to the acentric space group $P2_13$ [2]. This structure is composed of corner sharing ZrO_6 octahedra and WO_4 tetrahedra, but with an unusual aspect to the coordination of the WO_4 tetrahedra. While all the O atoms in the ZrO_6 octahedra are involved in Zr–O–W bonds with the WO_4 tetrahedra, only three of the four O atoms in each WO_4 tetrahedron are shared with Zr atoms. The fourth O atom is coordinated only to each W atom with a bond distance of about 0.17 nm. Pairs of WO_4 tetrahedra are arranged so that their terminal W–O bonds lie along lines orientated in $\langle 1\,1\,1\rangle$ directions. That bond points to the triangular base of the adjacent tetrahedron, but the O is about 2.4 nm away from the W in the adjacent tetrahedron, too far away to be considered bonded to it.

Above $T \approx 450$ K, β-ZrW_2O_8 has a disordered structure space group Pa3 [2]. The disorder in β-ZrW_2O_8 is associated with a random orientation of the terminal W–O bonds along a line parallel to the unit cell body diagonal. Oxygen mobility has been identified in the β-phase by dielectric and ac impedance measurements [2].

Cubic ZrW_2O_8 exhibits isotropic NTE both above and below the α–β phase transition. There is a continuous change in the lattice parameter near the order–disorder transition, with a significant reduction in volume of the unit cell in the high temperature phase [8]. NTE has been reported in the low temperature phase to as low as $T = 0.3$ K [1].

A third phase of ZrW_2O_8 (γ-ZrW_2O_8), having orthorhombic symmetry, has also been observed in a transition from the α-phase under pressures less than 0.2 GPa [9]. At $P = 0.2$ GPa the transformation is about 36 per cent complete and is 100 per cent complete at $P = 0.4$ GPa. This transition results in a unit cell volume reduction of 5 per cent. The phase is stable when the pressure is released, but can be converted back to the cubic form by heating at $T = 393$ K and ambient pressure.

While $ZrMo_2O_8$ polymorphs have been less well studied, cubic $ZrMo_2O_8$ also exhibits NTE behavior [5,7]. It is isostructural with the disordered β-phase of ZrW_2O_8; no transformation into a phase equivalent to the ordered phase of zirconium tungstate has been observed. Trigonal [10] and monoclinic forms [11] of $ZrMo_2O_8$ are also known but they do not show NTE. We note the potential for confusion in

the phase notations employing α and β, since several publications [12,13] identify the monoclinic phase as β-$ZrMo_2O_8$. In this paper cubic $ZrMo_2O_8$ refers to the disordered material isostructural with β-ZrW_2O_8.

While the specific heat of α-ZrW_2O_8 has been measured previously, the values have been obtained from either relaxation experiments [14] or calculated from vibrational densities of states [15–17]. Heat capacity measurements suitable for the generation of third-law entropies and use in Gibbs free energy calculations had not been reported in the literature at the time that we began our studies on either α-ZrW_2O_8 or cubic $ZrMo_2O_8$. In this paper, we report the results of semi-adiabatic calorimetric measurements at temperatures between (0.6 and 30) K and adiabatic calorimetric measurements between at temperatures between about 6 K and 400 K on both materials. During the preparation of this manuscript, we became aware of similar measurements conducted in the laboratories of Sorai [3,18] and Tsuji [19,20] on α-ZrW_2O_8.

2. Experimental

2.1. Sample preparation

The sample of α-ZrW_2O_8 was prepared at the Applied Materials Research Department, Lucent Technologies/Agere Systems, Murray Hill, NJ. The binary oxides {37.66 g of WO_3 (Alfa Aesar 99.998%) and 9.60 g ZrO_2 (Alfa Aesar 99.978%)} were vibratory milled for 18 h in methyl ethyl ketone using 270 g zirconia grinding media (residual mass loss of the media during milling was 0.53 g). The particle size after milling had a median diameter of 1 micron. An organic binder in methyl ethyl ketone was added (5 g) to promote compacting. The slurry was dried and pressed into pellets. The pellets were heated in oxygen by ramping the temperature slowly (14 $mK \cdot s^{-1}$) to $T = 523$ K to burn out the binder, then quickly to $T = 1470$ K (139 $mK \cdot s^{-1}$). The temperature was held at $T = 1470$ K for 4 h at which point the sample was rapidly quenched to room temperature in a stream of oxygen. The sample was below $T = 973$ K within 10 s. Complete transformation to ZrW_2O_8 is achieved by having small particle sizes, and decomposition into the binary oxides is minimized by fast quenching.

Cubic $ZrMo_2O_8$ was prepared in the Georgia Tech laboratories by dehydrating zirconium molybdenum oxide hydroxide hydrate. The hydrate was synthesized using the zirconyl perchlorate route which has been described previously [21].

2.2. Sample characterization

The chemical composition of both samples was determined at Brigham Young University using microprobe and X-ray fluorescence (XRF) techniques. The XRF technique (Siemens SRS 303) was used to scan qualitatively for a wide range of impurities. Wavelength dispersive spectroscopic (w.d.s) techniques on a Cameca XS-50 electron microprobe, operated at 20 kV with a current of 40 nA, were used to quantify those impurities significant enough to potentially affect the heat capacity.

No impurities were detected by XRF above the background level of the instrument for the tungstate sample. Any impurity that exists below the background level (several ppm) of the XRF would not be of significance to the heat capacity measurements. The molybdate sample was found to contain hafnium at a concentration of 0.45 mass per cent. Since the hafnium was present in the starting materials and since it can substitute for zirconium [22] we consider the best representation of the chemical formula of the calorimetric sample to be $Zr_{0.99}Hf_{0.01}Mo_2O_8$.

Both samples were characterized by powder X-ray diffraction (XRD) techniques. The powder pattern indicated the presence of the high pressure γ-ZrW_2O_8 phase at levels of 2 to 3 per cent. However, the sample, which was provided in hard pellets, was ground with an agate mortar and pestle before the diffraction pattern was taken. The pressures reached when the sample was ground are high enough to transform some of the sample to the high pressure γ-ZrW_2O_8 phase. The heat capacity measurements were performed prior to the XRD measurement and we believe that the sample was pure cubic α-ZrW_2O_8 before it was ground. A polished polycrystalline ceramic pellet of ZrW_2O_8 did not show any evidence of the high pressure phase by X-ray diffraction. No peaks associated with the starting materials were found within the limits of detection of the instrument. Rietveld analysis using GSAS software showed that the molybdate sample was contaminated with 1 per cent of the trigonal phase.

2.3. Calorimetric measurements

Measurements were performed using two different calorimetric techniques to cover the temperature range (0.6 to 400) K. Measurements made in the temperature range (6 to 400) K were taken on an adiabatic calorimeter of the Westrum design described previously in the literature [23–26]. In these experiments, we used a gold-plated calorimeter with a volume of 10.5 cm^3.

Temperatures were measured with a 25 Ω Pt resistance thermometer (SN 4253) manufactured by Rosemont Aerospace [27]. The thermometer was calibrated by the manufacturer over the range $13.8 \leqslant (T/\mathrm{K}) \leqslant 523$ on the ITS-90 temperature scale. The calibration was checked by measurement of the triple point of sodium sulfate dodecahydrate. Temperatures are believed to reproduce the ITS-90 to ±0.016 K for $13.8 < (T/\mathrm{K}) \leqslant 40$ K, and to ±0.005 K for $40 < (T/\mathrm{K}) \leqslant 523$. Calibration of the Pt thermometer below $T = 13.8$ K was performed against a germanium thermometer (SN 27277) manufactured by Lake Shore [28], and calibrated in-house against a rhodium-iron thermometer (SN B160) calibrated at the National Physical Laboratory in Teddington, UK, on the ITS-90 temperature scale. Below $T = 13.8$ K, the sensitivity of the platinum thermometer is reduced resulting in an estimated uncertainty in the temperature measurement of ±0.03 K.

Both samples were loaded into the adiabatic cryostat using a similar procedure. Each sample was placed in the calorimeter which was then evacuated on a vacuum line. A small pressure of helium gas was added to facilitate thermal conductivity and the calorimeter sealed by pressing a gold gasket against a knife edge. Because

the different synthetic procedures produced samples of different particle sizes and hygroscopicities, two differences in sample handling were followed prior to loading of the calorimetric vessel. The α-ZrW_2O_8 is not hygroscopic and was handled in air. The large pellets provided were broken into smaller pieces which could fit into the calorimeter. The cubic $ZrMo_2O_8$ was is hygroscopic and was handled exclusively in an argon-filled glove box whose water content was below 1 ppm. The sample was provided in powder form. In order to facilitate thermal conductivity, the sample was pressed into soft pellets with the pelletizing pressure kept well below 0.7 GPa, where cubic $ZrMo_2O_8$ is reported to undergo a first-order phase transition [4]. The pellets were loaded into the calorimeter which was transferred quickly to the vacuum line and evacuated. Details of the loading, including sample masses, helium gas pressure, and densities used in buoyancy corrections can be found in table 1.

The very low-temperature heat capacities were measured with an apparatus designed around a commercial ^{3}He insert capable of attaining temperatures as low as $T = 0.4$ K and with which measurements can be made as high as $T = 100$ K. Temperature increments are on the order of 10 per cent of the temperature. A similar apparatus has been described elsewhere [29] and further details of our apparatus have been recently described in the literature [30]. A Lake Shore Cernox 1030 thermometer [28] was used in the measurements from $0.5 \leqslant (T/\mathrm{K}) \leqslant 33$. This thermometer was calibrated in-house against the Tinsley [31] 100-Ω rhodium-iron thermometer (SN B160) described previously.

This instrument uses a semi-adiabatic pulse technique at low temperatures and an isothermal technique at higher temperatures. Usually the isothermal technique is used above $T = 10$ K since it requires less operator intervention. However, in these experiments, we used the semi-adiabatic technique up to $T = 30$ K because the thermal conductivity of our samples was poor and the isothermal technique gave unreliable results.

The same samples that were measured in the high temperature apparatus were used in the low temperature apparatus. Chunks of α-ZrW_2O_8 were attached directly to the platform using Apiezon–N grease. The cubic $ZrMo_2O_8$ could not be pressed at high enough pressures to form a good pellet without the possibility of a phase change so a ''putty'' method was devised to affix the sample to the platform. The sample was mixed with a known amount of Apiezon–N grease and placed in a copper cup. The copper cup was then fixed to the platform with Apiezon–N grease. The heat capacity of the addenda, copper cup (where applicable), and of Apiezon–N grease were measured separately and subtracted from the total specific heat to give the heat capacity of each sample. Details of the semi-adiabatic calorimetric experiments including masses of the samples, Apiezon–N grease, and copper cup are given in table 1.

Given the different operating parameters of the two cryostats, we are able to measure heat capacities on the same samples over the temperature regions that are optimal for each cryostat. We then combine the two sets of experimental results by inspecting the region of overlap and scale the low-temperature values so that they map smoothly onto the high-temperature values.

TABLE 1
Details of the calorimetric experiments for the adiabatic and semi-adiabatic measurements including sample mass M_s, mass of copper cup $M_{(Cu)}$ density ρ, and Molar mass M

	$6 < (T/\mathrm{K}) \leqslant 400$ Adiabatic measurements			
	α-ZrW_2O_8		cubic $ZrMo_2O_8$	
p(He gas)/kPa	1.87		3.06	
M_s/g	13.5992		7.3280	
$\rho/\mathrm{g \cdot cm^{-3}}$	5.076		3.5875	
Contribution of sample to measured C_p at selected T	T/K	$10^2 \cdot C_p(\alpha\text{-}ZrW_2O_8)/C_p(\mathrm{total})$	T/K	$10^2 \cdot C_p(\mathrm{cubic}\ ZrMo_2O_8)/C_p(\mathrm{total})$
	20	52	20	40
	200	25	200	21
	400	28	400	23
	$0.6 < (T/\mathrm{K}) \leqslant 30$ Semi-adiabatic measurements			
	α-ZrW_2O_8		cubic $ZrMo_2O_8$	
Apiezon–N/g	0.0044		0.1546	
M_s/g	0.8874		0.2009	
$M/\mathrm{g \cdot mol^{-1}}$	586.9192		411.1012	
M_{Cu}/g	NA		0.8086	
Contribution of sample to measured C_p at selected T	T/K	$10^2 \cdot C_p(\alpha\text{-}ZrW_2O_8)/C_p(\mathrm{total})$	T/K	$10^2 \cdot C_p(\mathrm{cubic}\ ZrMo_2O_8)/C_p(\mathrm{total})$
	1	10	1	5
	5	55	5	16
	10	74	10	20
	30	63	30	16

2.4. Corrections to the heat capacity measurements for impurities

No corrections to the heat capacity of the tungstate sample were made. The cubic $ZrMo_2O_8$ sample contains both chemical (Hf) and phase impurities (trigonal phase) for which corrections could be necessary. However, since no heat capacity measurements have been made of $(Zr, Hf)Mo_2O_8$ solid solutions, nor of the trigonal $ZrMo_2O_8$ phase, we lack the required data to make such calculations. Our results can be corrected at a later date, should this information become available. We note that the amount of trigonal phase formed depends highly on the dehydration process [21]. Our search of the literature indicates that our measurements have been on the best sample of cubic $ZrMo_2O_8$ prepared to date.

2.5. Estimates of the uncertainties of the measurements

Measurements of the standard molar heat capacity of synthetic sapphire (NIST SRM-720) were performed in the adiabatic apparatus in separate experiments in order to assess the accuracy of the heat capacity measurements obtained from this apparatus. We compared our results to those in table 2 of Archer [32] and found that our deviations are within the uncertainties quoted by Archer for his values. More details about the uncertainties of our sapphire measurements have been published previously [33,34]. In short, our sapphire measurements agree with those given in table 2 of Archer to within $\pm 0.02 \cdot C_p$ for $13 \leqslant (T/\mathrm{K}) < 25$; $\pm 0.005 \cdot C_p$ for $25 \leqslant (T/\mathrm{K}) < 30$; $\pm 0.002 \cdot C_p$ for $30 \leqslant (T/\mathrm{K}) < 40$; $\pm 0.001 \cdot C_p$ for $40 \leqslant (T/\mathrm{K}) < 250$; $\pm 0.0015 \cdot C_p$ for $250 \leqslant (T/\mathrm{K}) < 300$; and $\pm 0.001 \cdot C_p$ for $300 \leqslant (T/\mathrm{K}) < 400$. In each of the above ranges, our deviations are within the uncertainties quoted by Archer [32] for his values. The contributions of both samples to the total heat capacities are tabulated in table 1. We believe that the uncertainties for the measurements made on both calorimetric samples are within the stated uncertainties for synthetic sapphire. The inability to correct the measurements made on our slightly contaminated sample of cubic $ZrMo_2O_8$ for chemical and phase impurities implies that the reported results should be regarded as having a larger uncertainty with respect to the true values for a chemical and phase-pure sample of cubic $ZrMo_2O_8$. The uncertainties in the derived thermodynamic functions J at $T = 298.15$ K are estimated to be $0.002 \cdot J$ for the tungstate and $0.004 \cdot J$ for the molybdate.

The performance of the semi-adiabatic (low-temperature) apparatus was tested by measuring a single crystal of copper metal with a chemical purity of mass fraction .9999999. Below 30 K, the copper results were compared to the zero-field, low-temperature data of Holste *et al.* [35], Martin [36], and unpublished data of Phillips [37], and above $T = 30$ K the results were compared to additional measurements of Martin [38]. Our results fell within 0.5 per cent of the scatter obtained from the reference measurements, and our resolution was better than 0.1 per cent [30]. The contributions of the α-ZrW_2O_8 and cubic $ZrMo_2O_8$ to the total measured heat capacity are tabulated in table 1. The contributions of the cubic $ZrMo_2O_8$ were smaller than usual because of the copper cup and additional Apiezon–N grease that was used.

TABLE 2
Experimental molar heat capacities, $C^0_{p,m}$, of α-ZrW_2O_8 obtained with the adiabatic calorimeter. (M = 586.9192 g · mol^{-1})

T / K	$C^0_{p,m}$ / (J · K^{-1} · mol^{-1})	T / K	$C^0_{p,m}$ / (J · K^{-1} · mol^{-1})	T / K	$C^0_{p,m}$ / (J · K^{-1} · mol^{-1})
6.73*	0.695	60.73	63.71	154.99	148.05
7.54*	1.02	61.58	64.56	159.48	150.67
8.36*	1.47	61.95	65.38	160.10	150.84
10.18*	2.95	64.56	68.13	161.96	152.19
11.12*	3.71	65.42	69.02	164.59	153.62
11.71*	4.35	69.31	73.54	165.22	153.98
12.25*	5.05	70.18	74.57	167.08	155.06
12.76*	5.59	74.07	78.88	169.56	156.28
13.50*	6.00	74.94	79.84	170.35	156.91
13.80*	6.49	78.88	84.11	172.20	157.77
14.82*	7.92	79.76	85.10	174.68	159.02
14.94*	7.98	83.73	89.34	175.48	159.44
16.03*	9.16	84.62	90.50	177.33	160.63
16.25*	9.11	88.62	94.50	179.82	161.66
17.42*	10.32	89.52	95.55	180.61	162.09
17.70*	10.79	93.54	99.68	182.47	163.34
18.87*	12.25	94.44	100.56	184.95	164.21
19.32*	12.78	98.49	104.66	187.61	165.66
20.46*	14.08	99.40	105.36	190.09	166.54
22.26	16.58	103.47	109.20	192.64	167.73
22.98	17.49	104.38	110.07	192.75	167.98
24.22	19.03	108.46	113.66	195.24	168.95
26.34	21.67	109.38	114.70	197.77	170.12
28.69	24.72	113.48	118.04	197.89	170.54
31.27	27.92	114.40	118.92	200.38	171.46
34.13	31.32	118.82	122.69	202.91	172.31
35.67	33.53	119.43	123.18	203.03	172.82
37.27	35.51	123.85	126.63	205.35	173.42
38.77	37.34	124.48	127.09	205.53	173.51
42.08	41.48	128.91	130.39	208.06	174.59
45.64	45.88	129.54	130.94	208.18	174.96
47.12	47.63	133.98	134.14	210.50	175.67
49.25	49.94	134.61	134.62	210.68	175.73
50.78	52.05	139.07	137.85	213.22	176.65
54.45	56.51	139.70	138.10	213.33	177.11
54.45	56.51	144.16	141.12	215.65	177.83
55.82	57.74	144.79	141.46	218.36	178.83
57.86	60.36	149.26	144.52	218.48	179.23
58.18	60.90	149.88	145.03	220.80	179.92
58.68	61.12	154.36	147.72	223.52	180.97
223.64	181.33	277.77	200.39	311.32	211.00
225.94	182.14	280.28	201.16	313.95	211.92
228.68	182.97	280.34	201.79	315.36	212.01
231.10	184.05	280.37	201.75	316.49	212.42
233.86	184.82	282.94	202.36	319.12	213.53
236.28	185.78	284.35	202.29	320.54	213.66
239.02	186.77	285.45	202.97	321.66	213.98

TABLE 2 (*continued*)

T/K	$C^0_{p,m}$/(J · K^{-1} · mol^{-1})	T/K	$C^0_{p,m}$/(J · K^{-1} · mol^{-1})	T/K	$C^0_{p,m}$/(J · K^{-1} · mol^{-1})
241.44	187.73	285.50	203.26	324.31	215.12
244.18	188.62	285.54	203.37	325.72	215.09
246.60	189.65	288.12	203.87	326.83	215.58
249.34	190.45	289.52	203.69	329.49	216.68
251.77	191.58	290.62	204.66	330.89	216.60
251.92	191.86	290.68	205.14	332.00	216.91
254.45	192.46	290.71	205.20	334.66	218.42
254.50	192.50	293.27	205.58	336.08	218.18
256.93	193.36	293.29	205.51	337.18	218.58
257.08	193.13	294.68	205.59	339.84	219.55
259.62	194.72	295.78	206.29	341.28	219.59
259.65	194.44	295.86	206.77	342.35	220.29
262.09	195.39	295.89	206.53	345.02	221.11
262.25	195.51	298.42	207.35	346.48	221.34
264.79	196.32	298.46	206.87	347.53	221.22
264.80	196.31	299.83	207.34	350.20	222.57
267.26	197.40	300.96	207.99	352.71	223.20
267.43	197.08	301.06	208.00	357.89	224.66
269.96	198.07	303.59	208.75	363.07	226.80
270.05	198.43	303.64	208.71	368.25	227.91
272.42	198.84	305.01	209.09	373.43	229.76
272.60	199.02	306.15	209.38	378.61	231.41
275.12	199.47	306.23	209.90	383.80	233.41
275.16	199.91	308.78	210.46	390.00	234.91
275.20	199.97	310.18	210.45	394.19	236.97

*Data not included in the fit.

3. Results

The molar heat capacities of α-ZrW_2O_8 from the adiabatic apparatus and semi-adiabatic apparatus are reported in tables 2 and 3, respectively. The molar heat capacities of cubic $ZrMo_2O_8$ from the adiabatic apparatus and semi-adiabatic apparatus are reported in tables 4 and 5, respectively. An additional significant figure beyond those justified based on the uncertainties are given in the tables for those who might wish to perform numerical calculations on the results. In figure 1 the molar heat capacities of α-ZrW_2O_8 and cubic $ZrMo_2O_8$ obtained in this study in the region $20 < T/K < 400$ are presented, with the results for cubic $ZrMo_2O_8$ translated upwards by 10 J · K^{-1} · mol^{-1} for clarity. The results for $T/K < 30$ are shown in the insert to figure 1. The filled circles and squares represent data from the semi-adiabatic apparatus for α-ZrW_2O_8 and cubic $ZrMo_2O_8$, respectively. The triangles represent α-ZrW_2O_8 data from the adiabatic apparatus and the diamonds represent the cubic $ZrMo_2O_8$ data from the adiabatic apparatus. The unfilled triangles (α-ZrW_2O_8) and unfilled diamonds (cubic $ZrMo_2O_8$) represent data taken on the adiabatic apparatus that was not used in the data analysis described below.

TABLE 3
Experimental molar heat capacities, $C^0_{p,m}$, of α-ZrW_2O_8 obtained with the low temperature semi-adiabatic calorimeter ($M = 586.9192\ g \cdot mol^{-1}$)

T / K	$C^0_{p,m}$ / ($J \cdot K^{-1} \cdot mol^{-1}$)	T / K	$C^0_{p,m}$ / ($J \cdot K^{-1} \cdot mol^{-1}$)	T / K	$C^0_{p,m}$ / ($J \cdot K^{-1} \cdot mol^{-1}$)
0.603	0.00023806	1.442	0.0016553	4.087	0.077705
0.662	0.00032443	1.555	0.0024594	4.294	0.097905
0.662	0.00031382	1.556	0.0024662	4.500	0.12324
0.662	0.00032231	1.559	0.0021381	4.726	0.15549
0.726	0.00048902	1.565	0.0023433	4.950	0.19504
0.727	0.00040092	1.568	0.0024718	5.202	0.24546
0.727	0.00039498	1.709	0.0033179	5.447	0.30504
0.799	0.00053382	1.710	0.0032900	5.711	0.37583
0.799	0.00047501	1.710	0.0035258	5.994	0.46645
0.799	0.00059228	1.714	0.0030014	6.282	0.56659
0.800	0.00061269	1.721	0.0033261	6.593	0.69411
0.801	0.00060213	1.730	0.0034308	6.924	0.83961
0.879	0.00073142	1.815	0.0040623	7.255	1.0094
0.880	0.00065127	1.843	0.0043063	7.318	1.0371
0.880	0.00064737	1.879	0.0044794	7.622	1.2046
0.880	0.00057790	1.881	0.0044428	7.978	1.4241
0.881	0.00063451	1.882	0.0043927	8.064	1.4762
0.966	0.00097593	1.882	0.0042477	8.378	1.6757
0.966	0.00085484	1.901	0.0045266	8.775	1.9596
0.968	0.00076719	1.995	0.0052734	8.921	2.0617
0.969	0.00076180	2.052	0.0058590	9.220	2.2764
1.061	0.0012189	2.069	0.0059488	9.654	2.6277
1.063	0.0011101	2.070	0.0058924	9.812	2.7534
1.063	0.0010442	2.070	0.0058535	10.143	3.0158
1.063	0.0010486	2.076	0.0059994	10.625	3.4542
1.063	0.0009382	2.094	0.0060731	10.790	3.6004
1.169	0.0012736	2.199	0.0071133	11.867	4.6236
1.169	0.0012491	2.303	0.0081945	13.050	5.8144
1.170	0.0011613	2.418	0.0095202	14.328	7.1848
1.171	0.0011808	2.534	0.011068	15.764	8.8004
1.285	0.0015533	2.661	0.013081	17.357	10.6568
1.286	0.0014189	2.788	0.015371	19.086	12.7295
1.287	0.0014699	2.928	0.018323	20.993	15.0686
1.287	0.0014095	3.069	0.021983	23.111	17.7221
1.287	0.0012880	3.223	0.026618	25.402	20.5751
1.414	0.0017525	3.379	0.032526	27.897	23.6839
1.414	0.0017569	3.548	0.040059	30.669	27.1073
1.419	0.0014217	3.715	0.049556		
1.432	0.0018467	3.903	0.062169		

The standard molar thermodynamic functions, $C^0_{p,m}$, $\Delta^T_0 H^0_m$, $\Delta^T_0 S^0_m$, and $\Phi = \{\Delta^T_0 S^0_m - \Delta^T_0 H^0_m/T\}$ have been generated at smoothed temperatures by fitting appropriate mathematical functions to the experimental results. The results, scaled by the ideal gas constant, R, are given in tables 6 and 7, for the tungstate and molybate samples, respectively. Above $T = 4.0$ K for the tungstate and $T = 2.6$ K for the molybdate,

TABLE 4
Experimental molar heat capacities, $C^0_{p,m}$, of cubic $ZrMo_2O_8$ obtained with the adiabatic calorimeter. ($M = 411.1012\ g \cdot mol^{-1}$)

T / K	$C^0_{p,m}$ / ($J \cdot K^{-1} \cdot mol^{-1}$)	T / K	$C^0_{p,m}$ / ($J \cdot K^{-1} \cdot mol^{-1}$)	T / K	$C^0_{p,m}$ / ($J \cdot K^{-1} \cdot mol^{-1}$)
8.83*	1.20	105.88	109.37	255.26	196.18
9.94*	1.95	110.88	113.97	257.76	197.25
10.96*	2.36	115.90	118.51	260.42	198.47
11.73*	3.42	117.71	119.76	262.93	199.14
12.60*	4.58	120.94	122.69	265.58	200.18
13.64*	4.84	122.28	123.53	268.10	200.85
14.71*	6.66	125.99	126.73	270.74	201.90
15.90*	7.42	127.34	127.74	273.26	202.51
17.29*	8.82	132.41	131.63	275.92	203.44
18.85*	10.52	137.49	135.45	278.43	203.89
20.56*	12.83	142.58	139.01	281.09	205.06
22.45	15.03	147.67	142.51	283.61	205.53
24.55	17.40	152.77	145.87	288.79	207.12
26.84	20.13	157.88	149.16	293.97	208.67
29.36	23.31	163.00	152.40	299.13	210.22
30.68	25.06	168.12	155.60	299.97	210.53
32.13	26.75	173.24	158.46	304.30	211.90
33.37	28.34	178.38	161.46	305.01	212.21
36.22	31.87	180.44	162.67	309.48	213.23
39.26	35.50	183.51	164.18	310.19	213.69
42.56	39.51	185.60	165.47	314.65	214.70
46.11	43.83	188.65	166.89	315.34	215.28
49.70	48.17	190.74	168.27	317.60	215.41
53.35	52.50	193.79	169.78	320.52	216.56
55.70	55.36	195.88	170.97	322.65	217.23
57.06	56.87	198.93	172.67	322.73	216.73
57.72	57.30	201.01	173.72	327.83	218.54
59.50	59.83	206.15	176.34	327.91	218.04
62.25	62.74	211.31	178.74	329.99	218.39
63.28	64.22	216.46	181.16	333.01	219.84
66.92	67.90	221.61	183.41	333.09	219.71
67.09	68.65	226.76	185.56	335.00	220.01
71.64	73.32	231.92	187.59	336.07	220.72
74.82	77.18	237.08	189.59	338.18	221.44
76.42	78.71	242.24	191.44	338.27	221.60
81.24	84.03	245.00	192.70	339.99	221.30
86.11	89.40	247.41	193.35	343.36	222.64
91.01	94.50	250.10	194.50	343.47	222.17
95.94	99.72	252.57	195.07	344.95	222.39
100.90	104.60	252.61	195.16	346.44	223.43
348.54	223.96	359.01	225.79	374.35	230.17
348.66	223.41	359.35	225.91	377.01	230.90
349.90	223.68	359.74	226.42	379.17	231.53
351.63	224.83	363.79	227.46	381.39	231.85
353.72	225.12	364.18	227.80	383.98	232.78
353.83	224.43	364.63	227.70	385.77	232.67
354.83	224.76	368.21	228.75	388.78	233.73
354.90	224.81	369.50	228.55	390.12	233.86
358.91	226.56	372.62	229.66	394.45	235.22

*Data not included in the fit.

TABLE 5
Experimental molar heat capacities, $C^0_{p,m}$, of cubic $ZrMo_2O_8$ obtained with the low temperature semi-adiabatic calorimeter ($M = 411.1012\ g \cdot mol^{-1}$)

T/K	$C^0_{p,m}$/(J · K^{-1} · mol^{-1})	T/K	$C^0_{p,m}$/(J · K^{-1} · mol^{-1})	T/K	$C^0_{p,m}$/J · K^{-1} · mol^{-1}
0.601	0.001135	1.708	0.007761	8.112	1.524
0.602	0.001092	1.731	0.007706	8.489	1.754
0.658	0.001071	1.879	0.01035	8.778	1.896
0.661	0.001127	1.879	0.01026	8.916	1.988
0.727	0.001330	1.880	0.01032	9.337	2.278
0.728	0.001230	1.903	0.01038	9.662	2.455
0.798	0.001412	2.068	0.01359	9.800	2.565
0.800	0.001516	2.068	0.01400	10.249	2.851
0.879	0.001428	2.068	0.01408	10.625	3.108
0.879	0.001688	2.093	0.01426	10.775	3.195
0.880	0.001598	2.303	0.01954	11.299	3.678
0.968	0.001723	2.531	0.02739	11.857	4.091
0.968	0.001862	2.792	0.03848	12.401	4.495
1.063	0.002273	3.073	0.05466	13.034	5.038
1.064	0.002093	3.382	0.07715	14.348	6.306
1.168	0.002574	3.719	0.1106	15.781	7.684
1.169	0.002422	4.089	0.1576	16.517	8.425
1.169	0.002552	4.497	0.2205	17.359	9.314
1.285	0.002978	4.953	0.3149	18.161	10.19
1.285	0.003048	5.449	0.4376	19.079	11.09
1.286	0.003033	5.991	0.5986	19.966	11.91
1.414	0.003904	6.592	0.8147	20.984	13.16
1.552	0.005506	7.255	1.097	21.983	14.36
1.553	0.005742	7.370	1.145	23.081	15.82
1.553	0.005289	7.706	1.318	24.174	16.98
1.708	0.007814	7.980	1.455	25.382	18.31
1.708	0.007613				

orthogonal polynomials were fit to the experimental data. Below these temperatures, a combination of Debye and Einstein functions which adequately represent the data were used to extrapolate to 0 K and calculate the increments for the thermodynamic functions over these intervals. These functions have been used to model the low-energy vibrations in the negative thermal expansion materials and have been described elsewhere [39].

4. Discussion

The first reported molar heat capacity, $C_{p,m}$, of α-ZrW_2O_8, published by Ramirez and Kowach [14] was obtained from $1 < T/K < 300$ using a relaxation technique. Yamamura *et al.* [19] used adiabatic scanning calorimetry to measure the heat capacity in the vicinity of the order–disorder (α–β) transition above $T = 340$ K. Recently, measurements were made in the region $1.8 < T/K < 330$ using a commercial relax-

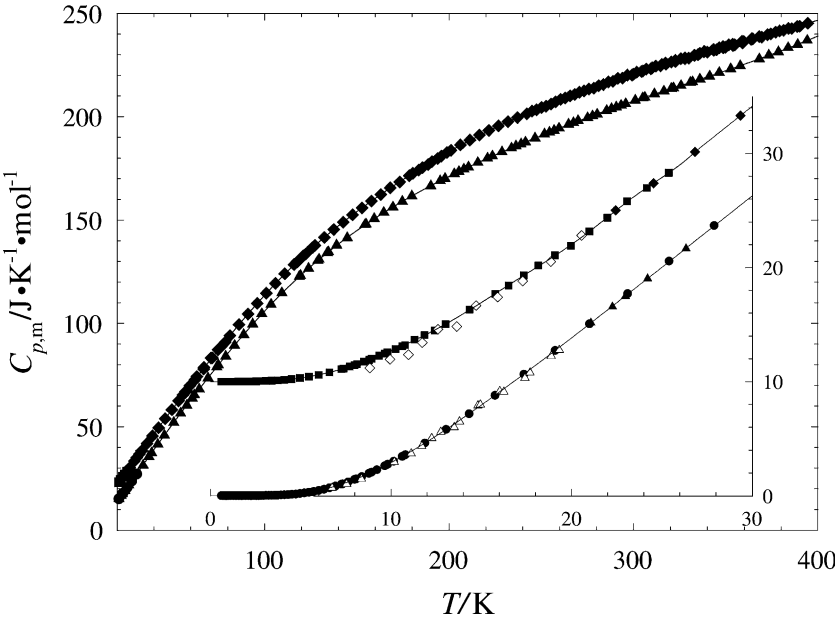

FIGURE 1. The experimental heat capacities of α-ZrW_2O_8 and cubic $ZrMo_2O_8$ as a function of temperature: α-ZrW_2O_8: ● semi-adiabatic apparatus, ▲ adiabatic apparatus; cubic $ZrMo_2O_8$: ■ semi-adiabatic apparatus, ◆ adiabatic apparatus. The results for cubic $ZrMo_2O_8$ have been shifted up by $10\ J \cdot K^{-1} \cdot mol^{-1}$ from the values reported in tables 4 and 5. The inset shows an expanded view of the low temperature results. The open triangles and diamonds in the inset are data taken on the adiabatic apparatus for α-ZrW_2O_8 and cubic $ZrMo_2O_8$ respectively, but not included in the fit. The solid curves, ——, represent heat capacities calculated from fits of the data.

ation calorimeter for data below $T = 10$ K and an adiabatic calorimeter for the higher temperatures [18]. Mittal and Chaplot [15,40] calculated the density of states using a semi-empirical interatomic potentials and generated the constant volume heat capacity, $C_{V,m}$, from them. We compare our results with these in figure 2.

The Ramirez and Kowach results [14] are consistently higher than all the other values, including ours. They are between 1 and 5 per cent higher than our data below $T = 100$ K, between 5 and 10 per cent higher in the range $100 < T/K < 200$, and about 10 per cent higher above $T = 200$ K. We suspect the large deviations of these results may arise from the limitations of the relaxation technique at high temperatures where radiation heat losses and other factors become important. Agreement between the BYU and unpublished results of Yamamura *et al.* [18,19] is much better. The deviations of our measurements with their results are within 1.5 per cent in the range $10 < T/K < 50$ and within 0.5 per cent in the range $50 < T/K < 320$.

We have corrected our calorimetric results ($C_{p,m}$) to $C_{V,m}$ using $C_{p,m} - C_{V,m} = \alpha_V^2 V_m T/\kappa_T$ to check for better agreement with the calculated heat capacities of Mittal and Chaplot [15,40]. The molar volume, V_m, and the volume coefficient of expansion, $\alpha_V = 1/V_m(\partial V_m/\partial T)_p$, was calculated from the temperature dependence of the lattice parameters obtained by Evans *et al.* [8] (Since the lattice is cubic, the volume

TABLE 6
Standard thermodynamic functions of α-ZrW_2O_8(cr) where, $\Phi^0_m = \Delta^T_0 S^0_m - \Delta^T_0 H^0_m/T$. $M = 586.9192$ g · mol^{-1}, $p^o = 100$ kPa and $R = 8.31451$ J · K^{-1} · mol^{-1}

T/K	$C^0_{p,m}/R$	$\Delta^T_0 S^0_m/R$	$\Delta^T_0 H^0_m/RT$	Φ^0_m/R
5	0.0245	0.005478	0.004385	0.001087
10	0.3499	0.099496	0.079171	0.017584
15	0.9550	0.34992	0.26545	0.0808105
20	1.6632	0.72033	0.52523	0.19100
25	2.4071	1.1713	0.82714	0.33978
30	3.1607	1.6768	1.1533	0.51895
35	3.9207	2.2211	1.4944	0.72206
40	4.6764	2.7940	1.8450	0.94431
45	5.4197	3.3879	2.2010	1.1821
50	6.1488	3.9967	2.5594	1.4324
60	7.5687	5.2441	3.2767	1.9625
70	8.9451	6.5146	3.9886	2.5210
80	10.275	7.7966	4.6918	3.0996
90	11.546	9.0809	5.3835	3.6922
100	12.740	10.360	6.0601	4.2945
110	13.848	11.627	6.7184	4.9031
120	14.866	12.876	7.3556	5.5152
130	15.796	14.103	7.9697	6.1283
140	16.648	15.306	8.5596	6.7406
150	17.431	16.481	9.1253	7.3506
160	18.154	17.629	9.6673	7.9571
170	18.825	18.750	10.186	8.5588
180	19.449	19.845	10.684	9.1552
190	20.034	20.912	11.161	9.7457
200	20.582	21.953	11.618	10.330
210	21.099	22.971	12.057	10.907
220	21.591	23.963	12.479	11.478
230	22.063	24.934	12.886	12.042
240	22.518	25.882	13.278	12.598
250	22.960	26.811	13.657	13.148
260	23.388	27.719	14.022	13.692
270	23.804	28.610	14.377	14.227
273.15	23.933	28.887	14.487	14.394
280	24.206	29.483	14.721	14.756
290	24.593	30.339	15.056	15.278
298.15	24.897	31.025	15.320	15.699
300	24.965	31.179	15.379	15.794
310	25.324	32.003	15.694	16.304
320	25.674	32.814	16.001	16.807
330	26.022	33.609	16.299	17.303
340	26.374	34.390	16.590	17.795
350	26.735	35.160	16.875	18.280
360	27.108	35.919	17.154	18.759
370	27.494	36.666	17.429	19.233
380	27.895	37.406	17.698	19.702
390	28.313	38.135	17.965	20.165
400	28.755	38.857	18.230	20.623

TABLE 7
Standard thermodynamic functions of cubic $ZrMo_2O_8$(cr), where $\Phi^0_m = \Delta^T_0 S^0_m - \Delta^T_0 H^0_m/T$. $M = 411.1012$ g · mol^{-1}, $p^o = 100$ kPa and $R = 8.31451$ J · K^{-1} · mol^{-1}

T/K	$C^0_{p,m}/R$	$\Delta^T_0 S^0_m/R$	$\Delta^T_0 H^0_m/RT$	Φ^0_m/R
5	0.02455	0.005478	0.004385	0.001087
10	0.3499	0.099496	0.079171	0.017584
15	0.9550	0.34992	0.26545	0.080811
20	1.6632	0.72033	0.52523	0.19100
25	2.4071	1.1713	0.82714	0.33978
30	3.1607	1.6768	1.1533	0.51895
35	3.9207	2.2211	1.4944	0.72206
40	4.6764	2.7940	1.8450	0.94431
45	5.4197	3.3879	2.2010	1.1821
50	6.1488	3.9967	2.5594	1.4324
60	7.5687	5.2441	3.2767	1.9625
70	8.9451	6.5146	3.9886	2.5210
80	10.275	7.7966	4.6918	3.0996
90	11.546	9.0809	5.3835	3.6922
100	12.740	10.360	6.0601	4.2945
110	13.848	11.627	6.7184	4.9031
120	14.866	12.876	7.3556	5.5152
130	15.796	14.103	7.9697	6.1283
140	16.648	15.306	8.5596	6.7406
150	17.431	16.481	9.1253	7.3506
160	18.154	17.629	9.6673	7.9571
170	18.825	18.750	10.186	8.5588
180	19.449	19.845	10.684	9.1552
190	20.034	20.912	11.161	9.7457
200	20.582	21.953	11.618	10.330
210	21.099	22.971	12.057	10.907
220	21.591	23.963	12.479	11.478
230	22.063	24.934	12.886	12.042
240	22.518	25.882	13.278	12.598
250	22.960	26.811	13.657	13.148
260	23.388	27.719	14.022	13.692
270	23.804	28.610	14.377	14.227
273.15	23.933	28.887	14.487	14.394
280	24.206	29.483	14.721	14.756
290	24.593	30.339	15.056	15.278
298.15	24.897	31.025	15.320	15.699
300	24.965	31.179	15.379	15.794
310	25.324	32.003	15.694	16.304
320	25.674	32.814	16.001	16.807
330	26.022	33.609	16.299	17.303
340	26.374	34.390	16.590	17.795
350	26.735	35.160	16.875	18.280
360	27.108	35.919	17.154	18.759
370	27.494	36.666	17.429	19.233
380	27.895	37.406	17.698	19.702
390	28.313	38.135	17.965	20.165
400	28.755	38.857	18.230	20.623

coefficient is three times that of the linear coefficient reported by Evans *et al.* [8]). We took the volume compressibility, $\kappa_T = -1/V_m(\partial V_m/\partial p)_T$, to be 0.0138 GPa^{-1} from the results of Jorgensen *et al.* [41]. Because of the large value of α_V, the $C_{p,m} - C_{V,m}$ correction becomes significant at temperatures as low as 100 K. With the correction, the values of $C_{V,m}$ calculated from the density of states are generally several per cent lower than our experimental results; these deviations are shown as an inset in figure 2. Evans *et al.* [8] note that the onset of the high temperature order–disorder transition is evident in the diffraction results as low as 250 K. Since the experimentally determined heat capacities contain contributions associated with that effect, the difference between our experimental values and the calculated ones may reflect the contribution of the order–disorder transition to the heat capacity in this region.

No literature results are available for comparison for the molybdate. The molybdate is reported to adopt the disordered cubic structure isomorphic to β-ZrW_2O_8 over the entire temperature range [5]. While there is some indication [7] that with slow cooling, ordering may take place below room temperature, we did not find any indication of a conversion throughout the time period of our measurements.

A comparison of the NTE materials with the sums of their respective binary oxides provides a qualitative look at the differences in the vibrational contributions

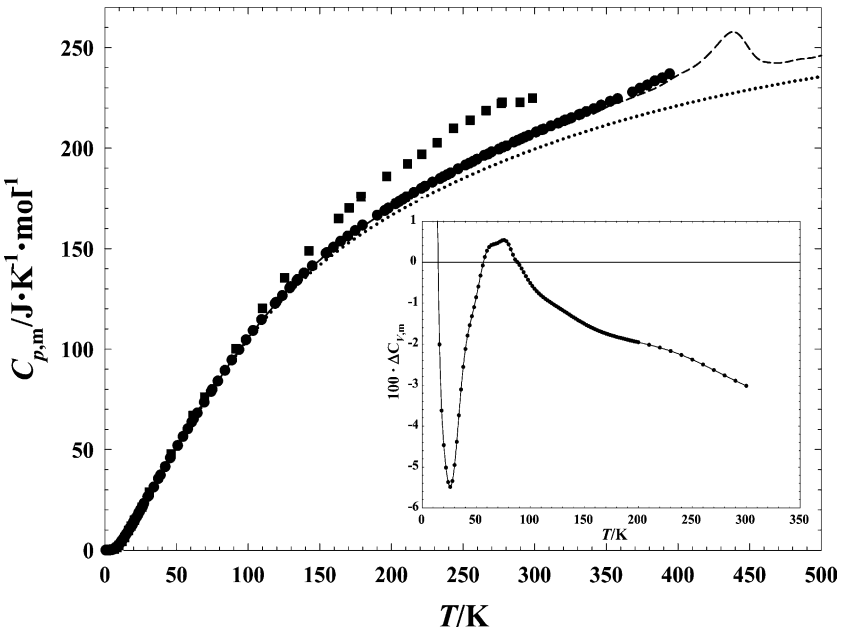

FIGURE 2. Comparison of the molar heat capacity of cubic ZrW_2O_8 obtained in this study with that reported in the literature: ●, This study; ■, Ramirez and Kowach, reference [14]; - - -, Yamamura *et al.*, reference [19]; ——, Yamamura *et al.*, reference [18]; ···, Mittal and Chaplot, references [15,40]. The inset shows the per cent deviations of our calculated $C_{V,m}$ to that of Mittal and Chaplot. The deviations are plotted as $100 \cdot \Delta C_{V,m}$ where $\Delta C_{V,m} = \{C_{V,m}(\text{Mittal}) - C_{V,m}(\text{this study})\}/C_{V,m}(\text{this study})$.

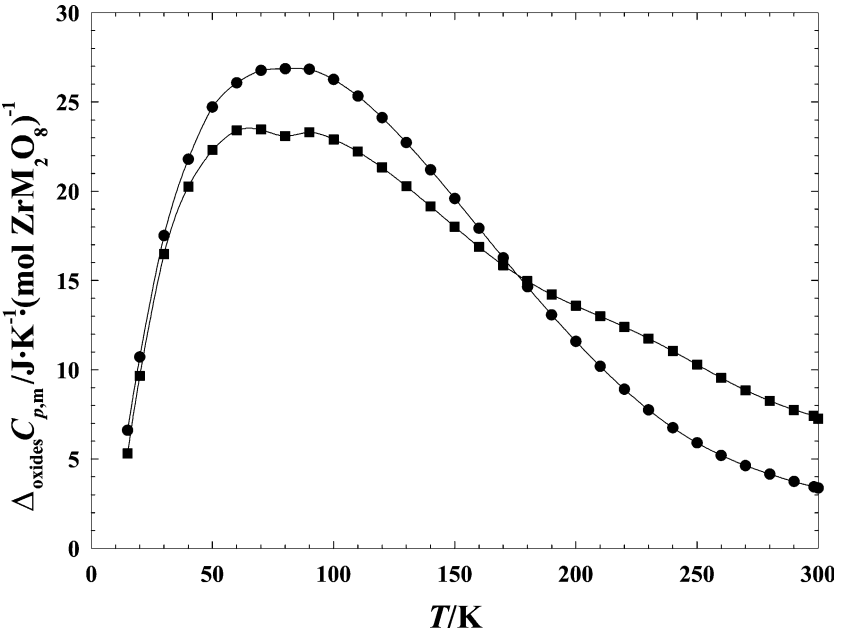

FIGURE 3. Heat capacity of the NTE material relative to the sum of the appropriate binary oxides: $\Delta_{\text{oxides}}C = C_{\text{p,m}}(\text{NTE}) - C_{\text{p,m}}(\text{ZrO}_2) - 2C_{\text{p,m}}(\text{WO}_3 \text{ or } \text{MoO}_3)$. ●, α-$ZrW_2O_8$; ■, cubic $ZrMo_2O_8$.

in the ternary oxides relative to those in the constituent binary oxides. We have measured the heat capacities [42] of MoO_3 and WO_3, for which good results below $T = 50$ K were not available, and used these results in combination with the recent heat capacities of ZrO_2 published by Atake *et al.* [43] to make the comparison. The excess heat capacity of the tungstate and molybdate relative to the sum of the binary oxides shows an unusually large positive value over the entire temperature range as shown in figure 3. Thus, one can infer the existence of a significant number of vibrational modes with lower frequencies in the negative thermal expansion materials relative to those in the binary oxides.

Acknowledgements

R. Stevens and J. Linford gratefully acknowledge financial support from the Office of Research and Creative Works at Brigham Young University. A.P. Wilkinson is grateful for financial support from the NSF (DMR-9623890) and the donors of the Petroleum Research Fund, administered by the American Chemical Society, under Contract No. 35087-AC5. We thank Professor Michael J. Dorais of BYU's Geology Department for his help with the microprobe and XRF analyses. We thank Professor T. Tsuji and Professor K. Saito for the provision of their unpublished results on α-ZrW_2O_8.

References

[1] T.A. Mary, J.S.O. Evans, T. Vogt, A.W. Sleight, Science 272 (1996) 90–92.
[2] J.S.O. Evans, T.A. Mary, T. Vogt, M.A. Subramanian, A.W. Sleight, Chem. Mater. 8 (1996) 2809–2823.
[3] Y. Yamamura, N. Nakajima, T. Tsuji, Y. Iwasa, K. Saito, M. Sorai, Solid State Commun. 121 (2002) 213–217.
[4] C. Lind, D.G. VanDerveer, A.P. Wilkinson, J. Chen, M.T. Vaughan, D. Weidner, Chem. Mater. 13 (2001) 487–490.
[5] C. Lind, A.P. Wilkinson, Z. Hu, S. Short, J.D. Jorgensen, Chem. Mater. 10 (1998) 2335–2337.
[6] N. Nakajima, Y. Yamamura, T. Tsuji, J. Therm. Anal. Calor. 70 (2002) 337–344.
[7] J.S.O. Evans, P.A. Hanson, R.M. Ibberson, N. Duan, U. Kameswari, A.W. Sleight, J. Am. Chem. Soc. 122 (2000) 8694–8699.
[8] J.S.O. Evans, W.I.F. David, A.W. Sleight, Acta Crystallogr. B 55 (1999) 333–340.
[9] J.S.O. Evans, Z. Hu, J.D. Jorgensen, D.N. Argyriou, S. Short, A.W. Sleight, Science 275 (1997) 61–65.
[10] M. Auray, M. Quarton, P. Tarte, Acta Crystallogra., Sect. C 42 (1986) 257–259.
[11] M. Auray, M. Quarton, P. Tarte, Powder Diffraction 2 (1987) 36–38.
[12] D.V.S. Muthu, B. Chen, J.M. Wrobel, A.M. Krogh Anderson, S. Carlson, M.B. Kruger, Phys. Rev. B 65 (2002) 064101.
[13] S. Carlson, A.M. Krogh Anderson, Phys. Rev. B 61 (2000) 11209–11212.
[14] A.P. Ramirez, G.R. Kowach, Phys. Rev. Lett. 80 (1998) 4903–4906.
[15] R. Mittal, S.L. Chaplot, Solid State Commun. 115 (2000) 319–322.
[16] G. Ernst, C. Broholm, G.R. Kowach, A.P. Ramirez, Nature (London) 396 (1998) 147–149.
[17] R. Mittal, S.L. Chaplot, H. Schober, T.A. Mary, Phys. Rev. Lett. 86 (2001) 4692–4695.
[18] Y. Yamamura, N. Nakajima, T. Tsuji, M. Koyano, Y. Iwasa, S. Katayama, K. Saito, M. Sorai, Phys. Rev. B 66 (2002) 014301.
[19] Y. Yamamura, N. Nakajima, T. Tsuji, Solid State Commun. 114 (2000) 453–455.
[20] Y. Yamamura, N. Nakajima, T. Tsuji, Phys. Rev. B 64 (2001) 184109.
[21] C. Lind, A.P. Wilkinson, C.J. Rawn, E.A. Payzant, J. Mater. Chem. 11 (2001) 3354–3359.
[22] C. Lind, Negative Thermal Expansion Materials Related to Cubic Zirconium Tungstate. Ph.D. Thesis, Georgia Institute of Technology: Atlanta, GA, 2001.
[23] J. Boerio-Goates, B.F. Woodfield, Can. J. Chem. 66 (1988) 645–650.
[24] E.H. Battley, R.L. Putnam, J. Boerio-Goates, Thermochim. Acta 298 (1997) 37–46.
[25] B.F. Woodfield, J. Boerio-Goates, J.L. Shapiro, R.L. Putnam, A. Navrotsky, J. Chem. Thermodyn. 31 (1999) 245–253.
[26] M.C. Beard, Heat capacity of α- and β-Silicon Nitride, D-ribose and modifications to low-temperature cryostat. M. S. Thesis, Brigham Young University: Provo, UT, 1998.
[27] Rosemont Aerospace, 12256 Trapp Road, Eagan, MN, 55121, USA.
[28] Lake Shore Cryotronics, Inc., 575 McCorkle Blvd., Westerville, OH, 43082, USA.
[29] B.F. Woodfield, Specific Heat of High-Temperature Superconductors: Apparatus and Measurement. Ph.D. Thesis, University of California, Berkeley:Berkeley, CA, 1995.
[30] J.C. Lashley, B.E. Lang, J. Boerio-Goates, B.F. Woodfield, T.W. Darling, F. Chu, A. Migliori, D. Thoma, J. Chem. Thermodyn. 34 (2002) 251–261.
[31] Tinsley Precision Instruments, 275 King Henry's Drive, New Addington, Cryodon, CR0 0AE, England.
[32] D.G. Archer, J. Phys. Chem. Ref. Data 22 (1993) 1441–1453.
[33] J. Boerio-Goates, M.R. Francis, R.N. Goldberg, M.A.V. Ribeiro da Silva, M.D.M.C. Ribeiro da Silva, Y.B. Tewari, J. Chem. Thermodyn. 33 (2001) 929–947.
[34] J. Boerio-Goates, R. Stevens, B.K. Hom, B.F. Woodfield, P.M. Piccione, M.E. Davis, A. Navrotsky, J. Chem. Thermodyn. 34 (2002) 205–227.
[35] J.C. Holste, T.C. Cetas, C.A. Swenson, Review of Scientific Instruments 43 (1972) 670–676.
[36] D.L. Martin, Phys. Rev. B 8 (1973) 5357–5360.

[37] N.E. Phillips, J.P. Emerson, R.A. Fisher, J.E. Gordon, B.F. Woodfield, D.A. Wright, unpublished data.
[38] D.L. Martin, Rev. Sci. Instrum. 58 (1987) 639–646.
[39] J. Boerio-Goates, R. Stevens, B. Lang, B.F. Woodfield, J. Therm. Anal. Calor. 69 (2002) 773–782.
[40] R. Mittal, S.L. Chaplot, Phys. Rev. B 46 (1999) 661–666.
[41] J.D. Jorgensen, Z. Hu, S. Teslic, D.N. Argyriou, S. Short, J.S.O. Evans, A.W. Sleight, Phys. Rev. B 59 (1999) 215–225.
[42] H.R. Catlin, R. Stevens, J. Linford, J. Boerio-Goates, J. Chem. Thermodyn., (in preparation).
[43] T. Tojo, T. Atake, T. Mori, H. Yamamura, J. Chem. Thermodyn. 31 (1999) 831–845.

02-013